AGU PUBLICATIONS

Journal of Advances in Modeling Earth Systems

RESEARCH ARTICLE
10.1002/2016MS000673

Scaling of the entropy budget with surface temperature in radiative-convective equilibrium

Martin S. Singh[1] and Paul A. O'Gorman[2]

[1]Department of Earth and Planetary Sciences, Harvard University, Cambridge, Massachusetts, USA, [2]Department of Earth, Atmospheric and Planetary Sciences, Massachusetts Institute of Technology, Cambridge, Massachusetts, USA

Key Points:
- Entropy budget of the atmosphere investigated in simulations of radiative-convective equilibrium at a wide range of surface temperatures
- Irreversible entropy sources from moist processes and friction increase with warming, but moist source does not scale with specific humidity
- Scaling relations constructed for terms in entropy budget are consistent with simulations but do not strongly constrain convective vigor

Correspondence to:
M. S. Singh,
martinsingh@fas.harvard.edu

Citation:
Singh, M. S., and P. A. O'Gorman (2016), Scaling of the entropy budget with surface temperature in radiative-convective equilibrium, *J. Adv. Model. Earth Syst.*, *8*, doi:10.1002/2016MS000673.

Received 18 MAR 2016
Accepted 6 JUN 2016
Accepted article online 9 JUN 2016

Abstract The entropy budget of the atmosphere is examined in simulations of radiative-convective equilibrium with a cloud-system resolving model over a wide range of surface temperatures from 281 to 311 K. Irreversible phase changes and the diffusion of water vapor account for more than half of the irreversible entropy production within the atmosphere, even in the coldest simulation. As the surface temperature is increased, the atmospheric radiative cooling rate increases, driving a greater entropy sink that must be matched by greater irreversible entropy production. The entropy production resulting from irreversible moist processes increases at a similar fractional rate as the entropy sink and at a lower rate than that implied by Clausius-Clapeyron scaling. This allows the entropy production from frictional drag on hydrometeors and on the atmospheric flow to also increase with warming, in contrast to recent results for simulations with global climate models in which the work output decreases with warming. A set of approximate scaling relations is introduced for the terms in the entropy budget as the surface temperature is varied, and many of the terms are found to scale with the mean surface precipitation rate. The entropy budget provides some insight into changes in frictional dissipation in response to warming or changes in model resolution, but it is argued that frictional dissipation is not closely linked to other measures of convective vigor.

1. Introduction

The steady state entropy budget of the atmosphere may be described as a balance between the net sink of entropy resulting from external heating and cooling and the net source of entropy owing to irreversible processes:

$$-\sum_i \frac{\mathcal{Q}_i}{T_i} = \dot{s}_{\mathrm{irr}}. \tag{1}$$

Here $\mathcal{Q}_i$ represents the external heat sources and sinks acting at temperatures T_i, and $\dot{s}_{\mathrm{irr}}$ is the total irreversible production of entropy by the atmosphere. In steady state, energetic balance requires that the external heat sources sum to zero (i.e., $\sum_i \mathcal{Q}_i = 0$), but since the atmosphere is heated from below and cooled aloft, the left-hand side of (1) is positive, ensuring that $\dot{s}_{\mathrm{irr}} \geq 0$ as required by the second law of thermodynamics.

Equation (1) has been applied to the global atmosphere, and a number of studies have diagnosed the global entropy budget based on observations [e.g., *Peixoto et al.*, 1991] and general circulation model (GCM) simulations [e.g., *Goody*, 2000; *Fraedrich and Lunkeit*, 2008; *Pascale et al.*, 2011]. A potential application of such analyses is in understanding model biases in the simulation of the global climate [*Johnson*, 1997; *Woollings and Thuburn*, 2006]. But GCMs do not resolve convective-scale motions, and moist processes associated with convection provide important irreversible sources of entropy in the atmosphere. Here we use simulations with an explicit representation of moist convection to examine the entropy budget of an atmosphere in the idealized state of radiative-convective equilibrium (RCE).

Previous authors have used the entropy budget of RCE [*Emanuel and Bister*, 1996] or related concepts based on a Carnot heat engine [*Rennó and Ingersoll*, 1996; *Craig*, 1996] in the construction of theories of moist-convective updraft velocity and buoyancy. These studies assume that frictional dissipation associated with atmospheric motions is the dominant irreversible entropy source in the atmosphere and thus may be

estimated by evaluating the left-hand side of (1). The dissipation rate is then related to the buoyancy and velocity of convective updrafts.

The above approach has been used successfully to estimate convective vigor in dry-convective layers, where frictional dissipation of atmospheric motions is indeed the dominant irreversible entropy source [see e.g., *Emanuel*, 2000]. In moist convection, however, frictional dissipation also occurs when hydrometers fall to Earth at their terminal velocity [*Pauluis et al*., 2000], and irreversible moist processes, including the mixing of dry and moist fluid parcels and nonequilibrium phase changes, are significant entropy sources that are not present in a dry atmosphere [*Pauluis and Held*, 2002a, 2002b]. The existence of these additional entropy sources reduces the ability of the atmosphere to generate kinetic energy [*Pauluis*, 2011], and only a small portion of the irreversible entropy production in a moist atmosphere is related to frictional dissipation resulting from atmospheric motions (termed anemonal dissipation by *Romps* [2008]). In order to use the entropy budget to estimate the anemonal dissipation rate, one must therefore also have detailed knowledge of the magnitude of these other irreversible entropy sources associated with moisture and precipitation. *Romps* [2008] analyzed the atmospheric budget of a quantity he denoted the "dry entropy" for which terms related to vapor diffusion and irreversible phase change do not appear explicitly. However, the net sink of dry entropy associated with the combination of radiation, condensation, and sensible heating is dependent on the profile of net condensation in the atmosphere, and this condensation profile may be sensitive to the diffusion and reevaporation of water vapor.

The importance of processes associated with moisture and precipitation for the irreversible production of entropy in the atmosphere suggests that the entropy budget may be strongly affected by a warming of the climate. At fixed relative humidity, the atmospheric concentration of water vapor increases approximately exponentially with temperature [following Clausius-Clapeyron (CC) scaling]. One may thus expect the importance of moist irreversible processes to also increase with warming, and this may have implications for the magnitude of the frictional dissipation rate under future climate change. Indeed, *Laliberté et al*. [2015] applied a heat-engine perspective to climate-model simulations of global warming and found that the power necessary to maintain the hydrological cycle increased following CC scaling, requiring decreases in work output to compensate. In steady state, the work output of the atmosphere must be balanced by the sum of the precipitation dissipation and the anemonal dissipation. Along similar lines, *Lucarini et al*. [2010] found decreases in work output in climate simulations as the value of the solar constant was increased, provided the control climate was sufficiently warm and moist. On the other hand, *Romps* [2008] reported an increase in the entropy sources associated with frictional dissipation under warming in simulations of RCE with a cloud-system resolving model (CRM).

In this study, we extend the work of *Pauluis and Held* [2002a, 2002b] and *Romps* [2008] by analyzing irreversible entropy production in a series of CRM simulations of RCE run over a much wider range of surface temperatures. We construct a set of simple scaling relations for the magnitude of various irreversible entropy sources in order to explain the behavior of the entropy budget as the atmosphere warms. The scaling relations are used to investigate the extent to which the entropy budget, coupled with simple reasoning regarding the behavior of moist processes, may provide insight as to the scaling of frictional dissipation (both total and anemonal) with warming. We also examine the relationship between the anemonal dissipation rate and the vigor of convection, as measured by, for example, the updraft velocity. A sensitivity analysis shows that the magnitudes of the simulated irreversible entropy sources are dependent on vertical resolution, potentially indicating the utility of the entropy budget in determining resolution requirements for deep moist convection.

The rest of this paper is organized as follows: we first outline the form of the entropy budget for dry and moist atmospheres (section 2) before we present the entropy budget of numerical simulations of RCE with a CRM (section 3). We then examine the scaling of the entropy budget over a range of surface temperatures, and we discuss the implications of the scaling results for our understanding of the behavior of moist convection (section 4). Finally, we analyze the relationship between the anemonal dissipation rate and the updraft velocity (section 5) before summarizing our conclusions (section 6).

2. Theory

Consider an atmosphere in RCE bounded below by a surface at fixed temperature in a horizontally homogenous and doubly periodic domain. We denote the net upward fluxes of short-wave and long-wave radiation

by F_{SW} and F_{LW}, respectively. The net radiative heating rate per unit volume is then given by $Q=-\partial_z(F_{SW}+F_{LW})$. For the purposes of this paper, it is sufficient to treat the radiative heating as externally applied so that the local entropy tendency per unit volume associated with radiative heating is given by Q/T, where T is the temperature [*Goody*, 2000]. (See *Stephens and O'Brien* [1993] for a treatment of the entropy production during the interaction of matter and radiation.) Similarly, the surface enthalpy flux F_H is associated with an entropy source given by F_H/T_s, where T_s is the surface temperature. The entropy budget (1) may then be written

$$-\int_S \left\{\frac{F_H}{T_s}\right\} \mathrm{d}S - \int_V \left\{\frac{Q}{T}\right\} \mathrm{d}V = \{\dot{s}_{\mathrm{irr}}\},$$

where the first integral is over the surface, the second integral is over the entire atmospheric volume, and the curly braces represent a time mean over sufficient duration that the time tendency of total entropy is negligible. In a statistical steady state, the surface enthalpy flux must balance the vertically integrated radiative cooling rate. Assuming T_s is constant, the above equation may then be simplified to

$$-\int_V \left\{Q\left(\frac{1}{T}-\frac{1}{T_s}\right)\right\} \mathrm{d}V = \{\dot{s}_{\mathrm{irr}}\}. \tag{2}$$

Diagnosis of the entropy budget requires the identification of the processes contributing to the total irreversible entropy production $\dot{s}_{\mathrm{irr}}$.

2.1. Dry Atmosphere

For the simple case of a dry atmosphere, the irreversible entropy sources include anemonal dissipation and the molecular diffusion of heat. In high Reynolds number flows typical of the atmosphere, the frictional term is dominant (see below) and we may write the entropy budget approximately as [e.g., *Emanuel*, 2000],

$$\langle -Q \rangle \left(\frac{1}{T_Q}-\frac{1}{T_s}\right) \approx \frac{\langle \mathcal{F} \rangle}{T_{\mathcal{F}}}.$$

Here $\mathcal{F}$ is the frictional dissipation rate, and the angle brackets denote a time average and volume integral per unit surface area given by

$$\langle \chi \rangle = \frac{1}{A}\int_V \{\chi\}\, \mathrm{d}V,$$

where A is the horizontal area of the domain. Additionally, we have defined effective temperatures $T_{\mathcal{F}}$ and T_Q by

$$T_\chi = \frac{\langle \chi \rangle}{\langle \chi/T \rangle}. \tag{3}$$

Given the radiative heating rate Q and the surface temperature T_s, one may use the assumption that the convective layer maintains a lapse rate close to dry-adiabatic to estimate T_Q. Lack of knowledge of the vertical profile of frictional dissipation limits the accuracy to which $T_{\mathcal{F}}$ may be estimated, but this still allows a reasonable estimate of $\langle \mathcal{F} \rangle$; the fractional error in $\langle \mathcal{F} \rangle$ depends only on the fractional error in $T_{\mathcal{F}}$.

In strongly forced systems, a further difficulty may arise because the temperature of the lower boundary is considerably different from the temperature of the atmosphere just above the molecular boundary layer through which the sensible heat flux is communicated by conduction. To be consistent with the neglect of the entropy production associated with molecular heat diffusion, the temperature used as T_s should be this low-level atmospheric temperature rather than the actual temperature of the boundary [e.g., *Romps*, 2008].

Notwithstanding the potential difficulties in accurately determining $T_{\mathcal{F}}$ and T_s, the above analysis shows how the simple framework of the steady state entropy budget may be used to determine the frictional dissipation rate in a dry-convecting layer given knowledge of the radiative cooling profile and boundary conditions. The dissipation rate, in turn, may be related to the vertical buoyancy flux and typical updraft velocities associated with dry convection [see e.g., *Emanuel et al.*, 1994].

2.2. Moist Atmosphere

In a moist atmosphere, (2) is still valid, but there are additional irreversible sources of entropy to consider. In particular, the frictional dissipation associated with falling precipitation [*Pauluis et al.*, 2000] and the irreversible entropy sources associated with diffusion of water vapor and phase changes under nonequilibrium conditions [*Pauluis and Held*, 2002a] must also be accounted for. The form of these various entropy sources may be derived from first principles using the Gibbs equation [*Raymond*, 2013], or, as emphasized by *Romps* [2008], by manipulating the governing equations traditionally used in numerical modeling. Here we simply give the result: assuming a steady state, the entropy budget of a moist atmosphere may be written

$$S = E_T + E_{\mathcal{F}} + E_P + E_{\mathcal{E}} + E_s + E_{\mathcal{M}} + E_D, \tag{4a}$$

where

$$S = \langle -Q \rangle (1/T_Q - 1/T_s), \tag{4b}$$

$$E_T = -\langle (\mathbf{D}_h \cdot \nabla T)/T^2 \rangle, \tag{4c}$$

$$E_{\mathcal{F}} = \langle \mathcal{F} \rangle / T_{\mathcal{F}}, \tag{4d}$$

$$E_P = g\langle P \rangle / T_P, \tag{4e}$$

$$E_{\mathcal{E}} = -R_v \langle \mathcal{E} \log\left(e/e_l^*\right) \rangle, \tag{4f}$$

$$E_s = -R_v \overline{\log\left(e_s/e_l^*\right) D_{vs}^z}, \tag{4g}$$

$$E_{\mathcal{M}} = R_v \langle \mathcal{M} \log\left(e_i^*/e_l^*\right) \rangle, \tag{4h}$$

$$E_D = -R_v \langle \mathbf{D}_v \cdot \nabla \log(e) \rangle. \tag{4i}$$

Equation (4a) may be derived from equation 26 of *Romps* [2008] under the conditions that the surface precipitation is entirely composed of liquid and the temperature of the air above the molecular surface layer, T_s, is constant. On the left-hand side of (4a), S is the net sink of entropy resulting from radiation and surface fluxes as defined by (4b). The right-hand side of (4a) represents various irreversible sources of entropy described below, and all terms are expressed per unit area of the domain.

Equations (4c)–(4e) describe irreversible entropy sources as a result of heat diffusion (E_T), anemonal dissipation ($E_{\mathcal{F}}$), and precipitation dissipation (E_P). The first two terms are present in the dry case; irreversible entropy production occurs when the kinetic energy of air motions is dissipated to heat, and when the diffusive flux of heat $\mathbf{D}_h$ is directed down the temperature gradient. The diffusive heat flux and the anemonal dissipation occur on molecular scales in the atmosphere, but in our simulations they will refer to the diffusion and dissipation produced by the model's subgrid scale parameterizations.

In the moist case, the irreversible loss of potential energy associated with the downward nonadvective flux of water, $P(x, y, z, t)$, leads to an extra source of entropy E_P. The rate of loss of potential energy by this process may be written $g\langle P \rangle$, where g is the gravitational acceleration. Dividing by the effective temperature T_P [defined as in (3)] then gives the associated entropy production. In the atmosphere, this entropy production occurs physically as a result of frictional dissipation in the shear zones surrounding falling hydrometeors, and P represents the precipitation flux. In our simulations, P also includes a component of vertical transport of water by subgrid scale turbulence, but because this component is small we refer to E_P as the entropy source owing to precipitation dissipation for simplicity. The work output in our simulations is given by the sum of the anemonal dissipation and precipitation dissipation [see (19)]. Heat diffusion between hydrometeors and the surrounding air is also a potential entropy source in the atmosphere [*Raymond*, 2013], but since the model we use does not allow the temperature of hydrometeors to differ from their surroundings, this source is absent in the simulations, and it is neglected in (4).

Equations (4f–4i) describe irreversible entropy sources as a result of evaporation at subsaturation in the atmosphere ($E_{\mathcal{E}}$) and at the surface (E_s), the melt-freeze cycle ($E_{\mathcal{M}}$), and diffusion of water vapor down the vapor-pressure gradient (E_D). Here R_v is the gas constant for water vapor, and e is the vapor pressure with saturation values over liquid of e_l^* and over ice of e_i^*. The evaporation rate is denoted by $\mathcal{E}$, with negative values corresponding to condensation, and the melting rate is denoted by $\mathcal{M}$, with negative values

corresponding to freezing. Sublimation can be taken as a combination of melting then evaporation. As with heat diffusion, the diffusive mass flux of water vapor $\mathbf{D}_v$ occurs on molecular scales in the atmosphere, but it is represented by the subgrid scale water-vapor transport in the CRM simulations. In (4g), D_v^z is the vertical component of this diffusive vapor flux with a value at the surface given by D_{vs}^z, the surface vapor pressure is denoted e_s, and the overbar represents a time and horizontal mean. In this notation $\overline{D_{vs}^z}$ represents the mean flux of water vapor into the atmosphere.

The terms described in (4f)–(4i) are associated with irreversible transformations of water substance, and we will refer to them collectively as the entropy source owing to moisture

$$E_m = E_{\mathcal{E}} + E_s + E_{\mathcal{M}} + E_D. \tag{5}$$

As originally found by *Pauluis and Held* [2002a, 2002b], the largest contributors to the moist entropy budget turn out to be the moisture terms E_m and the precipitation dissipation E_P.

3. Entropy Budget in CRM Simulations of RCE

We now analyze the components of the moist entropy budget (4) in simulations of RCE with a CRM. In this section we describe the model configuration and the entropy budget of a control simulation, and in the following section we consider the scaling of the entropy budget with surface temperature.

3.1. Model Configuration

We use a fully compressible and nonhydrostatic CRM similar to version 16 of the Bryan Cloud Model (CM1v16) [*Bryan and Fritsch*, 2002], which includes a parameterization of surface fluxes based on bulk-aerodynamic formulae and a band-averaged radiative transfer scheme. Cloud and precipitation microphysics are represented by a one-moment, six-species parameterization following *Lin et al*. [1983] (as updated by *Braun and Tao* [2000]) and identical to the "Lin-Hail" scheme described in *Singh and O'Gorman* [2014]. We include two separate representations of subgrid scale motions. First, a Smagorinsky scheme is used with separate diffusion coefficients in the horizontal and vertical [*Bryan and Rotunno*, 2009]. Second, we apply sixth-order hyper-diffusion to the velocity and humidity variables. This hyper-diffusion scheme is used in combination with a nondiffusive sixth-order advection scheme in order to limit the effect of implicit numerical diffusion on the simulated entropy budget. Both of the subgrid scale parameterizations must be considered in order to accurately calculate the subgrid scale fluxes (e.g., $\mathbf{D}_v$) when evaluating the entropy budget (4).

A number of alterations to the model were required in order to achieve accurate closure of the energy and entropy budgets. In particular, frictional heating associated with falling hydrometers is included in our simulations, while it is neglected in CM1v16. Additionally, alterations to the model's diffusion parameterization were required to ensure accurate conservation of water mass and accurate calculation of frictional heating resulting from anemonal dissipation. A complete description of the changes made to CM1v16 for this study may be found in *Singh* [2014]. (A number of these changes are included in CM1 version 17, released September 2013.) The imbalance in the energy budget of the resulting simulations, represented by the difference between the net atmospheric heating and the time tendency of the total energy of the atmosphere, is less than 1 W m^{-2} in most cases. Below we will show that these alterations also allow for approximate closure of the entropy budget.

We conduct a set of ten simulations of RCE with different imposed CO_2 concentrations in the range 1–640 ppm and corresponding fixed sea-surface temperature (SST) boundary conditions in the range 281–311 K. The boundary conditions used are derived from the equilibrium SSTs of a set of lower resolution, slab-ocean simulations run to steady state with the same range of CO_2 concentrations. Setting the SST in this way ensures that the radiative imbalance at the top of the atmosphere remains small ($<$3 W m^{-2}; Figure 1) despite the fact that the surface energy budget is not required to be closed. The simulations are conducted with a solar constant of 390 W m^{-2} and a zenith angle fixed to 43° so that there is no diurnal cycle of solar radiation. For simplicity, we do not impose a mean surface wind or any wind shear, with the result that the simulated convection does not show mesoscale organization.

The simulations are run with a horizontal grid-spacing of 1 km, a domain size of 84 $\times$ 84 km^2, and 64 vertical levels in which the vertical grid-spacing varies between 100 m near the surface and 500 m above 9 km. Each simulation is run for 40 days, and model output taken from the last 20 days is used in the analysis

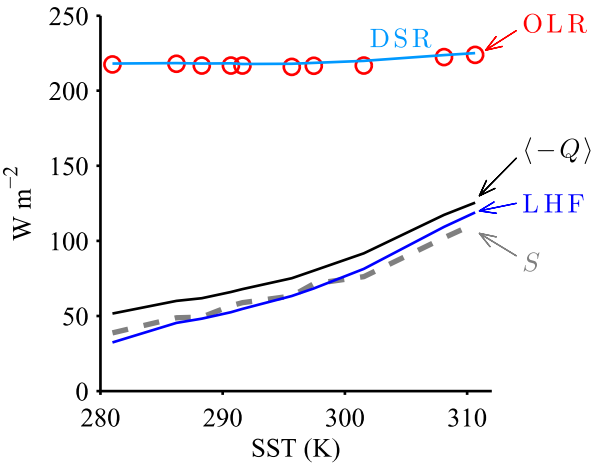

Figure 1. Outgoing long-wave radiation (OLR, red circles), net incoming short-wave radiation (DSR, light blue line), atmospheric radiative cooling rate ($\langle -Q \rangle$, black line), and surface latent heat flux (LHF, blue line) as a function of SST. Gray dashed line is proportional to entropy sink S, scaled to be equal to LHF at an SST of 295.7 K. All statistics are calculated using hourly snapshots from the final 20 days of each simulation.

below. The simulations are identical to the intermediate-resolution simulations described in *Singh and O'Gorman* [2014] and further details of the model configuration may be found there. In order to test the sensitivity of the results to horizontal resolution and domain size, we have repeated the simulations described above at a higher horizontal resolution (0.5 km grid-spacing) in a larger domain (160 $\times$ 160 km^2 domain) and found very similar results for the magnitudes of each entropy source. We do not focus on these high-horizontal-resolution simulations here because they exhibit larger trends in total entropy due to the shorter duration over which statistics are collected (10 days). We have also repeated a subset of the simulations with increased vertical resolution (256 levels) using the original horizontal grid-spacing (1 km) and domain size (84 $\times$ 84 km^2). The results for these high-vertical-resolution simulations are discussed in section 4.8.

3.2. Control Simulation

Table 1 gives the values of terms in the entropy budget in a simulation of RCE with an SST of 301.5 K, which we will refer to as the control simulation. These terms are calculated based on hourly snapshots from the last 20 days of the simulation and are expressed per unit horizontal area of the model domain. The entropy sink S is roughly equal to the sum of the irreversible sources (E_{tot}) given by the right-hand side of (4a), indicating that the entropy budget is approximately closed. The small difference between the entropy sink and E_{tot} is a result of the change in total entropy δs over the 20 day period in which statistics are gathered (approximately 7% of the size of E_{tot} as shown in Table 1), and truncation error in the model formulation or violation of the assumptions used to derive (4a). For instance, (4a) assumes all precipitation at the surface is in liquid form and that the value of T_s, identified here as the temperature at the lowest model level, is fixed.

Table 1. Terms in the Entropy Budget, Mean Surface Precipitation Rate, Effective Surface Relative Humidity, and Precipitation Efficiency for Control Simulation (CTRL) and High-Vertical-Resolution Simulation (HI-RES) With SST = 301.5 K

Description	Symbol	Equation	Units	CTRL	HI-RES
Entropy Budget					
Entropy sink	S	(4b)	mW m^{-2} K^{-1}	33.3	30.5
Total entropy source	E_{tot}		mW m^{-2} K^{-1}	34.1	33.1
Total entropy tendency	δs		mW m^{-2} K^{-1}	2.4	2.6
Error			mW m^{-2} K^{-1}	−1.5	0.1
Entropy Source Owing to					
Heat diffusion	E_T	(4c)	mW m^{-2} K^{-1}	−0.2	0.3
Anemonal dissipation	$E_{\mathcal{F}}$	(4d)	mW m^{-2} K^{-1}	5.3	6.7
Precipitation dissipation	E_P	(4e)	mW m^{-2} K^{-1}	10.8	11.3
Moisture	E_m	(5)	mW m^{-2} K^{-1}	18.3	14.8
Atmospheric evaporation	$E_{\mathcal{E}}$	(4f)	mW m^{-2} K^{-1}	3.2	3.2
Surface evaporation	E_s	(4g)	mW m^{-2} K^{-1}	3.5	3.2
Melt-freeze cycle	$E_{\mathcal{M}}$	(4h)	mW m^{-2} K^{-1}	2.7	2.6
Vapor diffusion	E_D	(4i)	mW m^{-2} K^{-1}	8.9	5.8
Mean vapor diffusion	$E_{\overline{D}}$	(12)	mW m^{-2} K^{-1}	5.2	1.0
Eddy vapor diffusion	$E_{D'}$	(13)	mW m^{-2} K^{-1}	3.7	4.8
Other Statistics					
Surface precipitation rate	$\overline{P_s}$		mm d^{-1}	2.89	2.96
Effective surface relative humidity	$\mathcal{R}_s$	(10)		0.80	0.82
Precipitation efficiency	ϵ_P			0.22	0.19

In the simulations, T_s is allowed to vary, and some frozen precipitation reaches the surface in simulations with lower SSTs to be shown below.

Temporal variations in entropy as measured by δs largely reflect variations in the entropy sink S. The entropy sources do not vary greatly in time, and the standard error for the estimates of each entropy source is less than 2% in all cases (standard error is estimated based on the values of each entropy source in 10 nonoverlapping subintervals of the model time integration). Therefore, even relatively small differences in individual entropy sources between simulations would be unlikely to occur as a result of sampling error alone.

The single largest irreversible source of entropy in the control simulation is that associated with frictional dissipation of falling precipitation, E_P. This term contributes roughly a third of the total irreversible entropy production, and it is twice as large as the entropy production owing to anemonal dissipation $E_{\mathcal{F}}$. The majority of the irreversible entropy production is not associated with frictional dissipation but rather results from irreversible entropy sources owing to moisture, which we have collectively referred to as E_m. The largest component of E_m is the entropy production associated with vapor diffusion E_D, but the entropy sources associated with phase changes are nonnegligible. As noted by *Pauluis and Held* [2002a], the distinction between entropy production resulting from vapor diffusion E_D and condensate reevaporation $E_{\mathcal{E}}$ is somewhat arbitrary in the atmosphere. Nevertheless, these terms may be separated in the context of the CRM simulations, and, as discussed further in the next section, their magnitudes scale somewhat differently as the surface temperature increases.

The dominance of E_m in the control simulation is consistent with the results of *Pauluis and Held* [2002a], although in that study ice processes were neglected, and the component of the entropy budget related to the melt-freeze cycle of atmospheric water did not appear. In our simulations, liquid water in the atmosphere often freezes well below 0°C, but ice does not melt until it experiences temperatures above 0°C. This difference in the mean freezing temperature and mean melting temperature results in an additional irreversible source of entropy $E_{\mathcal{M}}$ [*Romps*, 2008].

The remaining term in the entropy budget is the irreversible source of entropy associated with the diffusion of heat by the subgrid scale turbulence scheme E_T. This term is a small sink of entropy in the control simulation, suggesting heat is being diffused up the temperature gradient. As discussed by *Romps* [2008], such an up-gradient flux occurs because heat diffusion in the model is representing turbulent processes in which potential temperature, rather than temperature, is homogenized. In a stably stratified atmosphere, vertical diffusion of potential temperature is associated with up-gradient diffusion of temperature and is thus a sink of entropy. Since heat diffusion has a negligible impact on the overall entropy budget, however, we omit it from our discussion of the scaling of the entropy budget with temperature in the next section.

4. Scaling of the Entropy Budget With Surface Temperature

Figure 2 shows the simulated entropy budget as a function of SST. As for the control simulation, the differences between the entropy sink and the sum of the irreversible entropy sources are small, indicating approximate closure of the entropy budget. The component of this difference associated with temporal variations in total entropy δs and the component associated with model error are of the same order of magnitude (not shown).

The entropy sink increases with warming, varying by roughly a factor of 3 over the range of surface temperatures simulated. This rate of increase, while large, is substantially smaller than the fractional increase of the near-surface specific humidity representing Clausius-Clapeyron (CC) scaling (gray dashed line in Figure 2a) which increases by roughly a factor of 8 over the same range of temperatures. All of the irreversible entropy sources increase with warming except for $E_{\mathcal{M}}$ which increases and then decreases with warming (Figure 2b), and $E_{\mathcal{F}}$ which varies nonmonotonically but does increase over the full range of temperatures by a factor of roughly 1.5 (Figure 2a). The scaling of the irreversible entropy production owing to moisture E_m is similar to that of the entropy sink, although individual components of E_m increase at different fractional rates (Figure 2b). As a result of this sub-CC increase in E_m, the entropy budget is dominated by moist processes even at relatively low surface temperatures. The total frictional dissipation rate also increases strongly with warming, primarily as a result of a large increase in precipitation dissipation E_P.

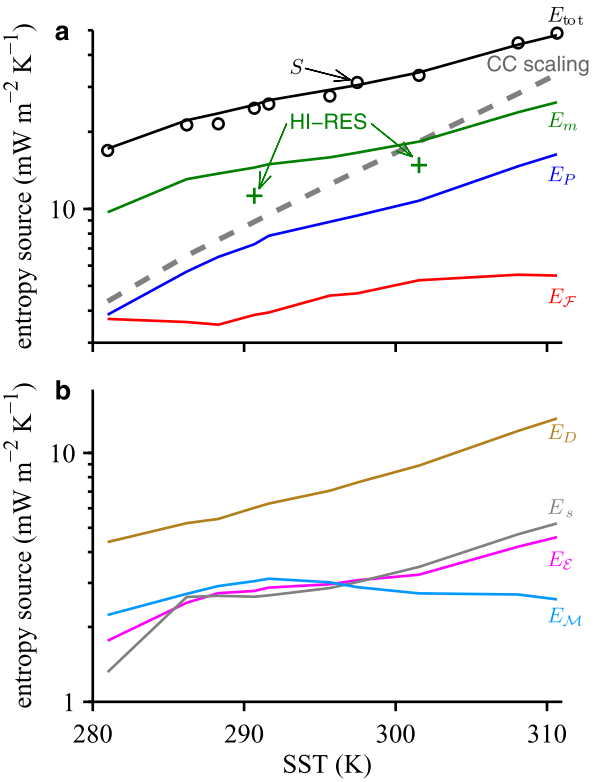

Figure 2. Entropy budget of RCE simulations as a function of SST. (a) Net entropy sink resulting from surface fluxes and radiative cooling of the atmosphere (S, black circles), irreversible sources of entropy owing to anemonal dissipation ($E_{\mathcal{F}}$; red line), frictional dissipation of falling precipitation (E_P; blue line), and moisture (E_m; green line), and the sum of all irreversible entropy sources (E_{tot}; black line). (b) Irreversible entropy production owing to moisture broken down into entropy production associated with evaporation within the atmosphere ($E_{\mathcal{E}}$; magenta) and at the surface (E_s; gray), the melt-freeze cycle ($E_{\mathcal{M}}$; light blue), and subgrid scale diffusion of water vapor (E_D; brown). In Figure 2a, green plus signs show entropy source owing to moisture E_m in high-vertical-resolution simulations (HI-RES), and the gray dashed line is proportional to the mean specific humidity at the lowest model level.

To better understand the variations in the entropy budget with temperature, we construct a set of approximate scalings for terms in the entropy budget as a function of surface temperature based on the simulations and equations (4b)–(4i). We consider the entropy sink and all the irreversible sources except for the entropy source resulting from heat diffusion E_T, which is negligible, and the entropy source owing to anemonal dissipation $E_{\mathcal{F}}$, which we return to in section 5. Our focus is on the overall scaling behavior over the range of surface temperatures simulated; our scaling relations will thus neglect second-order effects such as variations in relative humidity of the atmosphere with warming, which are shown to be relatively small in the simulations.

We first derive the scaling relations in sections 4.1–4.6 before evaluating their fidelity at reproducing the simulated entropy budget in section 4.7. Readers who are not interested in the derivation of the scalings may skip to section 4.7 where the scalings are summarized. We consider the effect of changes in vertical resolution on the simulated entropy budget in section 4.8.

4.1. Entropy Sink (S)

The magnitude of the sink of entropy S depends on the magnitude of the total radiative cooling of the atmosphere and the temperature at which this cooling occurs. A simple rearrangement of (4b) gives

$$S = \frac{\langle -Q \rangle}{T_Q} \left(\frac{\Delta T}{T_s} \right),$$

where $\Delta T = T_s - T_Q$. In steady state, the cooling rate $\langle -Q \rangle$ must be equal to the sum of the latent and sensible heat fluxes from the surface. In the simulations, the latent heat flux is generally dominant, and the latent heat flux is close to the value of $\langle -Q \rangle$ at high surface temperature (Figure 1). Furthermore, fractional changes in absolute temperature are relatively small even for the large variations in SST in the simulations, and Figure 3a shows that ΔT remains relatively constant as the surface temperature increases. As a result, the entropy sink S roughly scales with the latent heat flux as the atmosphere warms (Figure 1). In RCE, the surface evaporation rate is equal to the surface precipitation rate, and thus we may write a simple scaling for the entropy sink as

$$S \sim \overline{P_s}, \tag{6}$$

where P_s is the surface precipitation rate and the overbar represents a horizontal and time mean. As pointed out by a number of previous studies, the mean precipitation increases at a substantially lower fractional rate than the amount of atmospheric water vapor in response to greenhouse-gas induced warming [e.g., *Allen and Ingram*, 2002; *Held and Soden*, 2006]. Under the approximation (6), closure of the entropy budget requires that the total irreversible source of entropy must also scale with $\overline{P_s}$.

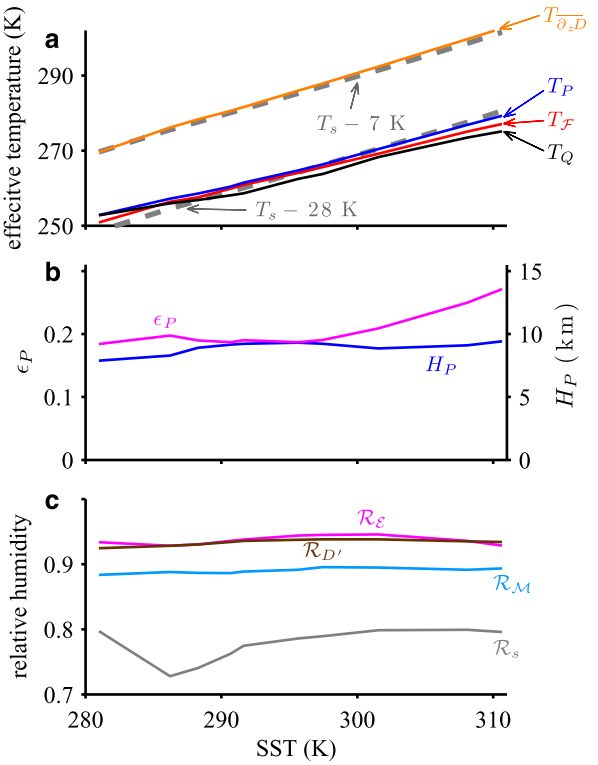

Figure 3. Properties of the simulations as a function of SST. (a) Effective temperatures of radiative cooling (T_Q; black), frictional dissipation ($T_{\mathcal{F}}$; red), precipitation dissipation (T_P; blue), and diffusive vapor flux divergence ($T_{\overline{\partial_z D}}$; orange) defined as in (3); T_s offset by 28 and 7 K is shown in gray dashed lines. (b) Precipitation efficiency (ϵ_P; magenta; left axis) and effective precipitation fall distance (H_P; blue; right axis). (c) Effective relative humidities $\mathcal{R}_{\mathcal{E}}$ (magenta), $\mathcal{R}_s$ (gray), $\mathcal{R}_{\mathcal{M}}$ (light blue), and $\mathcal{R}_{D'}$ (brown); see text for definitions.

4.2. Precipitation Dissipation (E_P)

The frictional dissipation associated with falling precipitation is equal to the rate of loss of gravitational potential energy as the hydrometeors fall $g\langle P\rangle$. If there were no evaporation of condensate, the integrated precipitation dissipation rate would be given simply by the surface precipitation rate multiplied by g and the mean height at which precipitation forms. More generally, we may define an effective precipitation fall distance, H_P, such that the integrated precipitation dissipation rate is $g\langle P\rangle = gH_P\overline{P_s}$ [*Pauluis et al.*, 2000]. In the no-evaporation case, H_P is the mean height of precipitation formation, but H_P is increased by the evaporation of falling hydrometeors.

With the definition above, the irreversible entropy source associated with falling precipitation E_P given in (4e) may be written,

$$E_P = \frac{gH_P\overline{P_s}}{T_P}, \tag{7}$$

where T_P is the effective temperature of falling precipitation. Fractional changes in T_P (Figure 3a) and H_P (Figure 3b), are relatively small and may be neglected in constructing the scaling. Then the entropy source associated with precipitation dissipation varies roughly in proportion to the mean surface precipitation rate,

$$E_P \sim \overline{P_s},$$

as in the case of the entropy sink above. Note that while we have derived the above scaling by only considering falling hydrometeors, P includes all nonadvective vertical transport of water, including water-vapor transport by subgrid scale diffusion, and this diffusion reduces E_P by roughly 8–9% in the simulations.

4.3. Evaporation in the Atmosphere ($E_{\mathcal{E}}$)

In the simulations, condensation of water vapor occurs at saturation, while the evaporation of hydrometeors may occur in subsaturated regions and contribute to the irreversible production of entropy. We may thus define an effective relative humidity $\mathcal{R}_{\mathcal{E}}$, so that the entropy source owing to evaporation in the atmosphere (4f) is

$$E_{\mathcal{E}} = -R_v\langle[\mathcal{E}]_+\rangle \log(\mathcal{R}_{\mathcal{E}}) \tag{8}$$

where $[\mathcal{E}]_+$ equals $\mathcal{E}$ when $\mathcal{E}$ is positive and zero otherwise. Recall that positive values of $\mathcal{E}$ correspond to evaporation and negative values correspond to condensation. The relative humidity $\mathcal{R}_{\mathcal{E}}$ thus represents a weighted average of the relative humidity during condensate evaporation.

The precipitation efficiency ϵ_P is defined as the ratio of the surface precipitation rate $\overline{P_s}$ to the total condensation rate $-\langle[\mathcal{E}]_-\rangle$, where $[\mathcal{E}]_-$ is equal to $\mathcal{E}$ when $\mathcal{E}$ is negative and zero otherwise. The surface precipitation rate is given by the net column condensation rate, $\overline{P_s} = -\langle[\mathcal{E}]_-\rangle - \langle[\mathcal{E}]_+\rangle$, and thus with a little rearrangement, the total evaporation rate may be expressed as

$$\langle [\mathcal{E}]_+ \rangle = \overline{P_s} \frac{(1-\epsilon_P)}{\epsilon_P}. \tag{9}$$

Combining (8) and (9), we may write the irreversible entropy production due to evaporation within the atmosphere $E_\mathcal{E}$ as

$$E_\mathcal{E} = -R_v \overline{P_s} \frac{(1-\epsilon_P)}{\epsilon_P} \log(\mathcal{R}_\mathcal{E}).$$

The precipitation efficiency ϵ_P remains roughly constant at a value of ≈ 0.2 at SSTs below ≈ 300 K, and then increases to ≈ 0.27 in the warmest simulation (Figure 3b). The effective relative humidity $\mathcal{R}_\mathcal{E}$ stays roughly constant at a value of ≈ 0.93 in all simulations (Figure 3c). Neglecting variations in both these quantities, the irreversible entropy production associated with evaporation within the atmosphere varies in proportion to the mean surface precipitation rate,

$$E_\mathcal{E} \sim \overline{P_s},$$

as for the previous terms considered.

4.4. Evaporation at the Surface (E_s)

The entropy production resulting from surface evaporation (4g) may be written in terms of an effective surface humidity $\mathcal{R}_s$ such that,

$$E_s = -R_v \overline{P_s} \log \mathcal{R}_s, \tag{10}$$

where we have again used that the mean surface precipitation rate $\overline{P_s}$ is equal to the mean surface evaporation rate $\overline{D_{vs}^z}$. If spatial and temporal variations in the surface relative humidity are not large, $\mathcal{R}_s$ will be approximately equal to the domain mean surface relative humidity. This is the case in the simulations where both $\mathcal{R}_s$ (Figure 3c) and the mean relative humidity in the lowest model level (not shown) remain between 0.7 and 0.8 at all SSTs. Neglecting the variations in $\mathcal{R}_s$ with SST, we have that the irreversible entropy production associated with surface evaporation scales with the mean precipitation rate,

$$E_s \sim \overline{P_s}.$$

4.5. Melt-Freeze Cycle ($E_\mathcal{M}$)

The entropy produced by the melting or freezing of a particle depends on the ratio of the saturation vapor pressures over liquid and solid at the temperature at which the phase change occurs [see (4h)]. In the model's thermodynamic formulation, the saturation vapor pressures above solid and liquid water are equal at a temperature of $T_0 = 273.15$ K, and thus only melting at temperatures above T_0 or freezing at temperatures below T_0 result in irreversible entropy production. In the simulations, melting typically occurs at temperatures close to T_0, although hail particles may remain frozen at temperatures several kelvins warmer. The formation of ice, however, occurs at temperatures as low as 233.15 K, resulting in a nonnegligible source of entropy. We define an effective "relative humidity" of freezing $\mathcal{R}_\mathcal{M}$ as a weighted average of the ratio of the saturation vapor pressures over solid and liquid during freezing (note that this ratio only depends on temperature). That is, $\mathcal{R}_\mathcal{M}$ is defined to satisfy

$$\left\langle \mathcal{M} \log\left(\frac{e_i^*}{e_l^*}\right) \right\rangle = \langle [\mathcal{M}]_- \rangle \log(\mathcal{R}_\mathcal{M}),$$

where $[\mathcal{M}]_-$ equals $\mathcal{M}$ when $\mathcal{M}$ is negative and zero otherwise. Recall that $\mathcal{M}$ is the microphysical tendency associated with the solid to liquid phase transition; $-\langle [\mathcal{M}]_- \rangle$ is the total mass rate of freezing occurring in the atmosphere. The entropy source associated with the melt-freeze cycle (4h) may then be written,

$$E_\mathcal{M} = R_v \langle [\mathcal{M}]_- \rangle \log(\mathcal{R}_\mathcal{M}).$$

The simulated mean freezing temperature does not vary greatly with surface warming, and as a result $\mathcal{R}_\mathcal{M}$ is also relatively constant across the simulations (Figure 3c). Thus, we may construct a scaling for the irreversible entropy source related to the melt-freeze cycle based on the total freezing rate in the atmosphere,

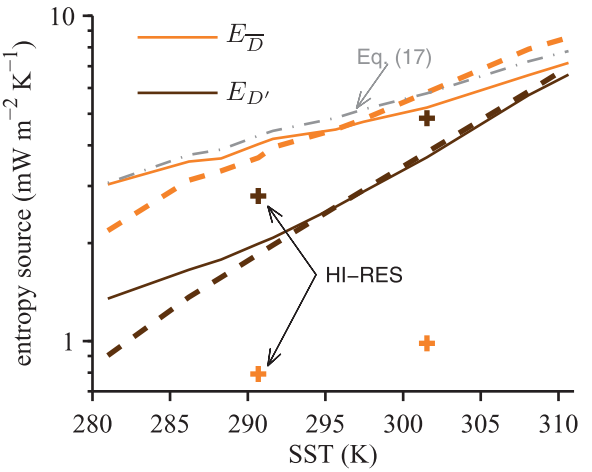

Figure 4. Irreversible sources of entropy owing to water-vapor diffusion down the mean gradient ($E_{\overline{D}}$; orange) and water-vapor diffusion associated with anomalies in the water-vapor field ($E_{D'}$; brown) for standard-vertical-resolution simulations (solid lines) and high-vertical-resolution simulations (plus signs). Scaling estimates based on (18f) (orange dashed line) and (18g) (brown dashed line) are shown with the scaled estimates set equal to the corresponding value in the standard-vertical-resolution simulation at an SST of 295.7 K. Dash dotted gray line shows estimate of $E_{\overline{D}}$ according to (17).

$$E_{\mathcal{M}} \sim -\langle [\mathcal{M}]_- \rangle. \tag{11}$$

Note that (11) requires knowledge of the total rate of freezing in the atmosphere, unlike the previous scalings, which only required knowledge of the mean surface precipitation rate.

4.6. Water-Vapor Diffusion (E_D)

We decompose the diffusion of water vapor into a mean component and an eddy component:

$$\mathbf{D}_v = \overline{D_v^z}\hat{\mathbf{k}} + \mathbf{D}'_v.$$

Here D_v^z is the vertical component of the diffusive flux of water vapor, $\hat{\mathbf{k}}$ is the unit vector in the vertical direction, the overbar represents a horizontal and time mean, and the prime represents an anomaly from this mean. This decomposition then allows for a similar decomposition of the entropy source owing to vapor diffusion (4i), $E_D = E_{\overline{D}} + E_{D'}$, where

$$E_{\overline{D}} = -R_v \left\langle \overline{D_v^z} \frac{\partial \overline{\log(e)}}{\partial z} \right\rangle, \tag{12}$$

$$E_{D'} = -R_v \langle \mathbf{D}'_v \cdot \nabla \log(e) \rangle. \tag{13}$$

The behavior of each of these terms as a function of SST is shown in Figure 4.

We first construct a scaling for $E_{D'}$. Neglecting the correlation between $\log(e)$ and the eddy component of the diffusive flux at the surface, we may use the divergence theorem to write,

$$E_{D'} = R_v \langle (\nabla \cdot \mathbf{D}'_v) \log(e) \rangle.$$

The above form for $E_{D'}$ may be divided into an integral over the regions where eddy diffusion is a sink of water vapor, and an integral over the regions where eddy diffusion is a source of water vapor,

$$E_{D'} = R_v \langle [\nabla \cdot \mathbf{D}'_v]_+ \log(e) \rangle + R_v \langle [\nabla \cdot \mathbf{D}'_v]_- \log(e) \rangle,$$

where, as before, $[x]_+$ equals x when x is positive and zero otherwise, and a similar definition applies to $[x]_-$. We define the effective vapor pressure of the sink regions e_+ by

$$\frac{\langle [\nabla \cdot \mathbf{D}'_v]_+ \log(e) \rangle}{\langle [\nabla \cdot \mathbf{D}'_v]_+ \rangle} = \log(e_+),$$

with a similar definition applying to the source regions to give e_-. By construction, the integrated sink of water vapor owing to the eddy component of vapor diffusion must be zero, and thus we may write

$$E_{D'} = -R_v \log\left(\frac{e_-}{e_+}\right) \langle [\nabla \cdot \mathbf{D}'_v]_+ \rangle. \tag{14}$$

Finally, we define an effective relative humidity $\mathcal{R}_{D'} = e_-/e_+$. To the extent that the eddy component of vapor diffusion primarily transports water vapor from cloudy (i.e., saturated) air to clear air, e_+ will be a weighted mean of the saturation vapor pressure and $\mathcal{R}_{D'}$ will represent a characteristic relative humidity at which diffusion moistens the environment.

Equation (14) shows that the entropy production associated with eddy diffusion is proportional to the magnitude of the eddy diffusive tendencies in the atmosphere. To estimate this term, we assume that the bulk

of the eddy diffusive transport of water vapor occurs at the boundary between clouds and clear air. Further, we assume that the diffusive flux of water vapor through the cloud boundaries scales with the humidity gradient at the cloud boundary, such that

$$\langle [\nabla \cdot \mathbf{D}_v{}']_+ \rangle \approx \rho \kappa \mathcal{A} |\nabla q_v|. \tag{15}$$

Here ρ is a characteristic value of the air density and $|\nabla q_v|$ is the magnitude of the specific humidity gradient at the cloud boundary. The parameter κ is a turbulent diffusivity and $\mathcal{A}$ represents the area of the cloud boundary per unit horizontal area of the model domain; these factors depend on the details of the turbulence at the boundaries of clouds [*Siebesma and Jonker*, 2000]. We can make some progress by assuming that the dominant effect of warming on (15) is the increase in the cloud-environment humidity gradient. For a constant environmental relative humidity, this gradient scales with the saturation specific humidity. Given that $\mathcal{R}_{D'}$ is only weakly dependent on the surface temperature (Figure 3c), we may then write a simple scaling for $E_{D'}$ as

$$E_{D'} \sim q_v^*. \tag{16}$$

Here q_v^* is a characteristic saturation specific humidity, which for simplicity we take to be the value near the surface (at the first model level). According to (16), the magnitude of the entropy source owing to eddy vapor diffusion follows CC scaling.

We now turn to the mean component of the entropy source owing to vapor diffusion given by (12). Neglecting vertical variations in relative humidity we have

$$E_{\overline{D}} \approx -R_v \left\langle \overline{D_v^z} \frac{\partial \overline{\log\left(e_l^*\right)}}{\partial z} \right\rangle.$$

Using the Clausius-Clapeyron relation, this may be written

$$E_{\overline{D}} \approx L_v \left\langle \overline{D_v^z} \frac{\partial}{\partial z} \left(\frac{1}{\overline{T}} \right) \right\rangle,$$

where L_v is the latent heat of vaporization, which we approximate as a constant for the purpose of this scaling. Integrating by parts in the vertical gives

$$E_{\overline{D}} \approx -L_v \frac{\overline{D_{vs}^z}}{T_s} - L_v \left\langle \frac{1}{\overline{T}} \frac{\partial \overline{D_v^z}}{\partial z} \right\rangle,$$

where we have neglected horizontal and temporal variations in T_s. Since the surface evaporative flux $\overline{D_{vs}^z}$ must be equal to the surface precipitation $\overline{P_s}$ in RCE, we may write an elegant approximation for $E_{\overline{D}}$,

$$E_{\overline{D}} \approx L_v \overline{P_s} \left(\frac{1}{T_{\overline{\partial_z D}}} - \frac{1}{T_s} \right), \tag{17}$$

where $T_{\overline{\partial_z D}}$ is the effective temperature at which the atmosphere is moistened by the mean vertical diffusive flux of water vapor [defined as in (3)].

In Earth's atmosphere, nonadvective water-vapor transport is achieved by molecular diffusion. For the net vertical transport of water vapor, this is only significant in the molecular boundary layer near the surface. As a result, we would expect $T_{\overline{\partial_z D}} \approx T_s$, and $E_{\overline{D}} \approx 0$. But in the simulations, subgrid scale fluxes produce substantial net vertical transports of water vapor through a large portion of the lower troposphere, and $T_{\overline{\partial_z D}}$ is roughly 7 K lower than T_s (Figure 3a). The term $E_{\overline{D}}$ is thus a significant component of the simulated entropy budget but has no counterpart in Earth's atmosphere. We explore this limitation of the simulations in section 4.8.

A simple scaling for $E_{\overline{D}}$ may be constructed by assuming the factor involving T_s and $T_{\overline{\partial_z D}}$ in (17) is roughly constant with warming, such that

$$E_{\overline{D}} \sim \overline{P_s}.$$

However, since $\Delta T_D = T_s - T_{\overline{\partial_z D}}$ is relatively small (compared to, e.g., $\Delta T = T_s - T_Q$), this scaling is particularly sensitive to variations in ΔT_D as a result of, for example, changes in the lapse rate with warming.

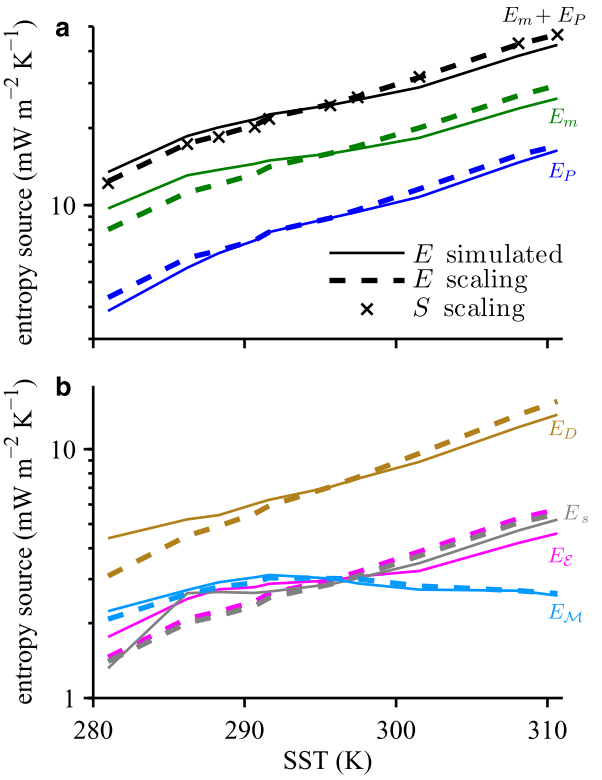

Figure 5. As in Figure 2 but showing approximate scalings (dashed lines) for each term based on equations (18b)–(18g) and neglecting $E_\mathcal{F}$. The scaling estimates are set equal to the corresponding simulated values at an SST of 295.7 K. (a) Black lines show the sum of irreversible entropy sources $E_m + E_P$ according to the simulations (solid) and scalings (dashed), and black crosses show the scaling for the entropy sink based on (18a) set equal to the value of $S - E_\mathcal{F}$ at 295.7 K. (b) The scaling for E_D is determined by summing the scalings for $E_{\overline{D}}$ (18f) and $E_{D'}$ (18g).

4.7. Evaluation of Scaling Relations

We have derived a series of approximate scaling relations for terms in the entropy budget as a function of surface temperature which may be summarized as follows,

$$S \sim \overline{P_s}, \tag{18a}$$

$$E_P \sim \overline{P_s}, \tag{18b}$$

$$E_\mathcal{E} \sim \overline{P_s}, \tag{18c}$$

$$E_s \sim \overline{P_s}, \tag{18d}$$

$$E_\mathcal{M} \sim -\langle [\mathcal{M}]_- \rangle, \tag{18e}$$

$$E_{\overline{D}} \sim \overline{P_s}, \tag{18f}$$

$$E_{D'} \sim q_v^*. \tag{18g}$$

According to (18), the entropy sink and the irreversible entropy sources owing to precipitation dissipation, evaporation, and diffusion down the mean vapor gradient all scale with the mean precipitation rate $\overline{P_s}$. The two terms that deviate from this scaling behavior are the entropy sources associated with the melt-freeze cycle and eddy vapor diffusion.

Despite the approximations used in their derivation, the scaling relations roughly reproduce the entropy budget in the CRM simulations. The dashed lines in Figure 5 show the magnitude of terms in the entropy budget assuming they vary with surface temperature according to (18) and are equal to the corresponding simulated values at an SST of 295.7 K. The nonmonotonic variation of $E_\mathcal{M}$ is captured, which implies that this variation is related to an increase and then a decrease in the total freezing rate as the atmosphere warms. The scaling also captures the behavior of $E_{D'}$ for moderate and high surface temperatures, although the rate of increase is overestimated at low surface temperatures (Figure 4). The scaling overestimates the increase in $E_{\overline{D}}$, and the approximation (17) that includes the variation of $T_{\frac{-1}{\partial_z \overline{D}}} - T_s^{-1}$ is more accurate (Figure 4).

The reasonable agreement between the scaling relations and the simulated entropy budget is possible because the relative humidity structure, precipitation efficiency, precipitation fall distance, and temperature differences such as $\Delta T = T_s - T_Q$ remain relatively constant as the surface temperature increases. It is possible that these quantities may be more sensitive to warming outside of the idealized state of RCE considered here.

Neglecting the influence of anemonal dissipation, the scaling relations are broadly consistent with a closed entropy budget over the range of surface temperatures considered (compare the black crosses and black dashed line in Figure 5a). This is the case even though $E_\mathcal{M}$ and $E_{D'}$ do not scale with $\overline{P_s}$; the smaller fractional changes in $E_\mathcal{M}$ are compensated for by the larger fractional increases in $E_{D'}$. At even higher surface temperatures, this compensation would be unlikely to hold, and either $E_{D'}$ would no longer follow CC scaling or some change to the scaling of the other irreversible entropy sources would be required to ensure closure of the entropy budget.

If the scaling relationships were completely accurate, the above results would imply that the entropy production associated with anemonal dissipation $E_\mathcal{F}$ also scales with the surface precipitation rate in order for the entropy budget to close. But the scaling relations only reproduce the simulated entropy budget

approximately. Since the entropy source $E_{\mathcal{F}}$ is only a small fraction of the entropy sink, inaccuracies in the scaling relations lead to large errors in the estimate of the anemonal dissipation, and, in practice, (18) provides only weak guidance as to the scaling of anemonal dissipation with warming.

The behavior of the scaling relations and simulations contrast with the recent study of *Laliberté et al*. [2015], which found a decrease in the work output of the global atmosphere under climate warming, implying a decrease in the sum of the anemonal and precipitation dissipation. In our simulations, the precipitation dissipation scales roughly with the precipitation rate itself, and as a result, the total dissipation increases strongly with warming. Such an increase in the dissipation is possible because the entropy source owing to moisture E_m also scales roughly with the precipitation rate. A higher rate of increase of E_m with warming (e.g., if E_m were to follow CC scaling) would require a smaller increase or a decrease in the frictional dissipation rate in order for the entropy budget to close.

4.8. Sensitivity to Vertical Resolution

As pointed out in section 4.6, the entropy source associated with mean vapor diffusion $E_{\overline{D}}$ is likely overestimated in our simulations. This may diminish the importance of the eddy component $E_{D'}$ in the entropy budget, and, since $E_{\overline{D}}$ and $E_{D'}$ scale somewhat differently with warming, it may affect the scaling of E_m with temperature. We test the sensitivity of the magnitude of $E_{\overline{D}}$ to model formulation by repeating the control simulation (SST = 301.5 K) at a higher vertical resolution (HI-RES), with 4 times the number of vertical levels, keeping the horizontal resolution and domain size fixed. In the HI-RES case, a longer simulation (60 days, statistics collected over last 40 days) was found to be required to sufficiently reduce the time tendency of total entropy δs (Table 1). The HI-RES simulation is similar to the control in many respects, including having a similar mean precipitation rate, precipitation efficiency, and surface relative humidity. However, the entropy source owing to mean vapor diffusion is reduced by a factor of 5 in HI-RES. This may be understood as follows. As the vertical grid-spacing Δz is made smaller, the turbulent diffusion coefficients in the model's subgrid scale parameterizations also decrease since more of the turbulence is explicitly resolved. This reduction occurs in the Smagorinsky scheme, which has separate diffusion coefficients in the horizontal and vertical, as well as in the sixth-order hyper-diffusion scheme, which has a vertical hyper-diffusion coefficient that is proportional to Δz^6. On the other hand, the mean vertical gradients of specific humidity and water-vapor pressure are relatively unaffected by the change in Δz. The net vertical diffusive flux of water vapor is thus smaller at higher vertical resolution, and since the vertical vapor-pressure gradient remains unchanged, $E_{\overline{D}}$ decreases with decreasing Δz.

The reduction in $E_{\overline{D}}$ in the HI-RES simulation is compensated for by an increase in entropy sources associated with anemonal dissipation, eddy vapor diffusion, precipitation dissipation, and heat diffusion, although the total entropy source does decrease slightly (Table 1). The increase in the precipitation dissipation and heat diffusion terms is primarily a result of the decreased importance of vertical diffusion in the HI-RES simulation. Recall that the vertical transport of water vapor by diffusion is included in the calculation of P; it reduces E_P by $\sim$1 mW m^{-2} K^{-1} in the control simulation but by only $\sim$0.1 mW m^{-2} K^{-1} in HI-RES. Similarly, the entropy sink associated with heat diffusion in the control simulation becomes a source in HI-RES because the entropy sink owing to vertical diffusion of potential temperature is reduced in magnitude relative to the source from horizontal diffusion.

In contrast to the precipitation dissipation and heat diffusion terms, the increased entropy sources associated with eddy vapor diffusion $E_{D'}$ and anemonal dissipation $E_{\mathcal{F}}$ in HI-RES are not simple consequences of the change in vertical grid-spacing. The entropy budget may thus provide a useful pathway for understanding the sensitivity of simulated moist convection to resolution changes. For instance, the anemonal dissipation rate is roughly 25% higher in HI-RES compared to the control, potentially pointing to the importance of vertical resolution for properly representing turbulence associated with moist convection. This increase may be qualitatively understood as arising from the requirement of a closed entropy budget given the reduction in parameterized vertical diffusion.

While $E_{D'}$ contributes a larger fraction of the total irreversible entropy production in HI-RES than in the control, the difference is likely to be too small to strongly affect the scaling of the total entropy source owing to moisture E_m. This is confirmed by conducting a second high-vertical-resolution simulation at an SST of

290.7 K; $E_{D'}$ becomes the dominant contributor to E_D when the vertical resolution is increased (Figure 4), but this change only marginally influences the scaling of E_m with temperature (Figure 2a, green plus signs).

5. Anemonal Dissipation and the Vigor of Moist Convection

Previous work on the entropy budget of moist convection has focused on the anemonal dissipation rate and its associated entropy source as a measure of convective vigor. The results described above suggest that the entropy budget provides some insight into the behavior of the anemonal dissipation rate with warming and with changes in resolution, even if a strong quantitative constraint remains difficult to obtain. However, it is unclear to what extent the anemonal dissipation rate may be related to more familiar concepts relating to convective vigor such as the updraft velocity. In this section, we briefly examine the relationship between updrafts and anemonal dissipation in the RCE simulations.

The integrated kinetic energy budget in a moist atmosphere may be written

$$-\langle \mathbf{u} \cdot \nabla p \rangle = \langle \mathcal{F} \rangle + g\langle P \rangle, \tag{19}$$

where $\mathbf{u}$ is the velocity, p is the pressure, and the left-hand side represents the work done by the atmosphere [see *Romps*, 2008, equation (18)]. By mass conservation, the downward nonadvective flux of water must be balanced by an upward advective flux of moist air, $\langle P \rangle = \langle \rho w \rangle$, where ρ is the density and w is the vertical velocity. Furthermore, making the hydrostatic approximation we have $\nabla p \approx -\bar{\rho} g \hat{\mathbf{k}}$. Substituting these expressions into (19) allows us to write

$$\langle \mathcal{F} \rangle \approx g\langle \bar{\rho} w \rangle - g\langle \rho w \rangle.$$

The above equation expresses a balance between anemonal dissipation and the production of kinetic energy by buoyancy forces. The irreversible entropy source owing to anemonal dissipation (4d) may then be written

$$E_{\mathcal{F}} \approx \frac{\langle \bar{\rho} w b \rangle}{T_{\mathcal{F}}}, \tag{20}$$

where $b = g(\bar{\rho} - \rho)/\bar{\rho}$ is the buoyancy. While strict equality in (20) only occurs for a hydrostatic atmosphere, it is a good approximation in the RCE simulations.

In the absence of drag and nonhydrostatic pressure gradients, a parcel of air accelerated upward by a buoyancy force B over a depth H will obtain a vertical velocity $w = \sqrt{2BH}$. This suggests a scaling for the buoyancy flux of the form $\langle \bar{\rho} w b \rangle = \langle \rho \rangle W^3/H$, where W is a characteristic vertical velocity and H is the depth of the troposphere. Combining this scaling with (20), we may write

$$W \approx \left(\frac{E_{\mathcal{F}} T_{\mathcal{F}} H}{\langle \rho \rangle} \right)^{\frac{1}{3}}. \tag{21}$$

Taking H to be the height of the tropopause (defined as the level at which the lapse rate is equal to 2 K km^{-1}), we may use the simulated values of $E_{\mathcal{F}}$ and the effective temperature $T_{\mathcal{F}}$ (Figure 3a) to estimate W; it increases by a factor of $\sim$1.5 over the range of surface temperatures simulated. This is broadly consistent with the behavior of the root-mean-squared vertical velocity

$$w_{\mathrm{RMS}} = \left(\frac{\langle \bar{\rho} w^2 \rangle}{\langle \rho \rangle} \right)^{1/2}, \tag{22}$$

which increases by a factor of 1.7 across the simulations. However, the value of w_{RMS} is less than 0.3 m s^{-1} in all the simulations, an order of magnitude smaller than the vertical velocities typically associated with cloud updrafts in simulations [*Robe and Emanuel*, 1996] and observations [*LeMone and Zipser*, 1980] of deep convection. A more relevant statistic for intense updrafts is obtained by calculating the 99.99th percentile of the vertical velocity distribution at each model level and taking the maximum value of this 99.99th percentile profile. This measure of updraft velocity, which we denote w_{max}, increases with warming from 7 to 16 m s^{-1} across the simulations [see also *Singh and O'Gorman*, 2015, Figure 2]. This is an increase by a factor of $\sim$2.3, somewhat larger than the factor of 1.5 implied by the scaling based on the anemonal dissipation

Table 2. Measures of the Vertical Velocity (m s^{-1}) in Simulations with 64 Vertical Levels (the Standard Vertical Resolution) and 256 Vertical Levels (HI-RES) for Two Different SSTs[a]

			SST = 290.7 K		SST = 301.5 K	
Vertical Velocity Measure	Symbol	Equation	64-Level	256-Level	64-Level	256-Level
$E_{\mathcal{F}}$-based scaling	W	(21)	1.07	1.22	1.29	1.38
Root-mean-squared	w_{RMS}	(22)	0.20	0.22	0.25	0.27
Peak of 99.99th percentile	w_{max}		9.0	8.2	12.4	13.0

[a]The standard error owing to sampling uncertainty was estimated as in section 3.2 and was found to be less than 2% for each vertical velocity measure.

rate. Additionally, w_{max} responds differently to increases in vertical resolution than either W or w_{RMS}. In the high-vertical-resolution simulations, both W and the root-mean-squared velocity w_{RMS} are increased relative to the corresponding lower resolution cases (Table 2). The effect on w_{max}, however, depends on the SST, with w_{max} increasing with increasing vertical resolution for the 301.5 K simulations and decreasing with increasing vertical resolution for the 290.7 K case. The anemonal dissipation rate thus does not provide guidance as to how vertical resolution affects strong updrafts in our simulations.

The difficulty of using the anemonal dissipation rate to predict updraft velocities comes about because small vertical velocities make a large contribution to the vertical buoyancy flux in some simulations. This may be seen by considering the function

$$F_b(\hat{w}) = \langle \bar{\rho} w b \delta(|w| - \hat{w}) \rangle,$$

which describes how the integrated vertical buoyancy flux $\langle \bar{\rho} w b \rangle$ is distributed among vertical motions with different speeds. Here δ is the Dirac delta function and $F_b(\hat{w})\, \mathrm{d}\hat{w}$ describes the buoyancy flux resulting from vertical motions with speeds (both upward and downward) in the infinitesimal interval $(\hat{w}, \hat{w} + \mathrm{d}\hat{w})$. Figure 6 shows the values of F_b in the simulations estimated using 50 discrete bins, with bin widths varying from 0.01 m s^{-1} at $|w| = 0$ m s^{-1} to 1 m s^{-1} at $|w| = 25$ m s^{-1}. As the atmosphere warms, the proportion of the integrated vertical buoyancy flux that is contributed by strong vertical motions increases substantially (Figure 6a). For instance, in the coldest simulation, updrafts and downdrafts with speeds above 7 m s^{-1} contribute negligibly to the buoyancy flux, while for the warmest simulation ~50% of the buoyancy flux is effected by such rapid vertical motions. On the other hand, the increase in the buoyancy flux associated with an increase in vertical resolution is mainly evident at weak vertical speeds; for the simulations with an SST of 301.5 K, the buoyancy flux associated with vertical motions of speeds $|w| > 5$ m s^{-1} is almost identical in the high-vertical-resolution and standard-vertical-resolution cases (Figure 6b).

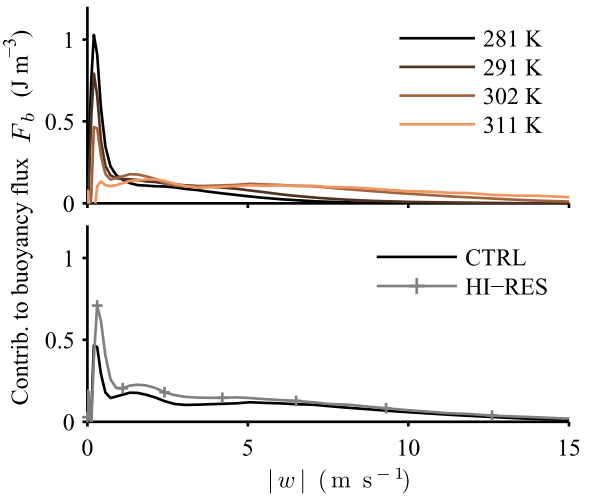

Figure 6. The function F_b, which describes the contribution to the buoyancy flux of vertical motions with different magnitudes. (a) Standard-vertical-resolution simulations at different SSTs shown in the legend and (b) standard-vertical-resolution (black line) and high-vertical-resolution (gray line with plus signs) simulations at an SST of 301.5 K. See text for definition of F_b.

The importance of relatively weak vertical motions for the behavior of the integrated buoyancy flux suggests that the anemonal dissipation rate provides limited insight into the behavior of cloud updrafts in moist convection, particularly if one is interested in the upper tail of the vertical velocity distribution. A more promising alternative is to reason directly about the buoyancy of clouds in an atmosphere that is constrained to remain close to neutral to the most entraining elements in the convective ensemble [*Singh and O'Gorman*, 2013; *Seeley and Romps*, 2015]. Such an approach was recently used with some success in understanding the behavior of updraft velocities under warming in *Singh and O'Gorman* [2015].

6. Conclusions

We have investigated the entropy budget of moist convection in a series of simulations of radiative-convective equilibrium over a wide range of surface temperatures. As found previously by *Pauluis and Held* [2002a] for tropical surface temperatures, processes associated with transformations of water substance and the fall of precipitation are responsible for the bulk of the irreversible entropy production in the atmosphere, even in the coldest simulation. We find that the magnitudes of both the irreversible entropy production owing to moisture and the entropy production associated with frictional dissipation increase with warming. In contrast, *Laliberté et al*. [2015] analyzed the atmospheric heat engine in a global climate model and argued that Clausius-Clapeyron scaling of the power required to maintain the hydrological cycle implies that the work performed by the atmosphere decreases under global warming; in the long-term average, the work output must be equal to the total (precipitation and anemonal) dissipation rate. A similar decrease in work output was reported by *Lucarini et al*. [2010] for present-day Earth-like conditions in simulations of warming induced by increases in the solar constant.

In our simulations, the magnitude of the irreversible entropy production owing to moisture does not increase as rapidly as the specific humidity, but rather it scales roughly with the surface precipitation rate. This allows for an increase in the frictional dissipation rate with warming [see also *Romps*, 2008]. One possible reason for these differing results is the differing spatial scales of interest. *Laliberté et al*. [2015] argued that their heat-engine analysis should be seen as applying to large-scale motions rather than motions associated with convection. In addition, large-scale horizontal temperature gradients may play an important role in the global entropy budget. For instance, *Knietzsch et al*. [2015] found decreases in frictional dissipation along with decreases in the pole-to-equator temperature gradient in GCM simulations in which the magnitude of a specified ocean heat transport was increased. In our study, moist convection is the focus, and large-scale motions and horizontal temperature gradients are not considered. A second possible reason for the differing results is that *Laliberté et al*. [2015] and *Lucarini et al*. [2010] used a global climate model with parameterized moist convection that may not properly represent moist processes such as precipitation dissipation that are important to the entropy budget. In our simulations, an increase in work output is required to allow for the large increase in precipitation dissipation that occurs with warming.

We further investigated the dependence of the entropy budget on surface temperature by constructing a set of approximate scalings that relate the magnitude of terms in the entropy budget to diagnostics such as the mean precipitation rate, freezing rate, and near-surface specific humidity. The scaling relations are based on a number of simplifying assumptions including that the relative humidity distribution, precipitation efficiency, and precipitation fall distance remain invariant under warming, but they nevertheless approximately reproduce the temperature dependence of terms within the entropy budget of the simulations. While the scaling relations do not include an estimate of the behavior of the entropy production associated with anemonal dissipation, they are consistent with an increase in the precipitation dissipation rate with warming, and precipitation dissipation corresponds to the bulk of the frictional dissipation in the atmosphere.

Previous work on the entropy budget of moist convection has sought to derive a constraint on the anemonal dissipation rate as a measure of convective vigor [e.g., *Emanuel and Bister*, 1996]. In principle, the scaling relations in combination with the requirement for a closed entropy budget allows one to estimate the scaling of anemonal dissipation with warming. Due to the approximate nature of the scaling relations, however, such an estimate provides only a qualitative guide to the behavior of the simulations. Furthermore, the behavior of cloud updrafts may not be simply related to the anemonal dissipation; in our simulations, strong updrafts increase in magnitude with warming to a greater extent than would be suggested by a scaling based on the anemonal dissipation rate. These results highlight the difficulty in deriving insights regarding convective vigor from considerations of the entropy budget of a moist atmosphere.

A potential use of the entropy budget is to understand how artificial diffusion or subgrid schemes affect convection in numerical models. For instance, we find that the magnitude of the simulated entropy source owing to vapor diffusion down the mean gradient is sensitive to the model's vertical resolution. At high vertical resolution, the mean vapor diffusion plays a smaller role in the entropy budget, consistent with the expectation that such diffusion is negligible for convection in Earth's atmosphere. The reduction in entropy production associated with vapor diffusion is compensated, in part, by an increase in the entropy

production associated with anemonal dissipation. The entropy budget thus provides a framework for understanding the effect of vertical resolution on turbulence associated with moist convection.

The results presented here focus only on disaggregated convection with no large-scale organization. But simulations of RCE are known to spontaneously develop convective organization in a process known as self-aggregation [*Bretherton et al*., 2005]. Furthermore, when rotation is included, such aggregation may result in tropical cyclone formation [*Wing et al*., 2016], potentially leading to an increase in work output and a decrease in inefficiencies associated with moist processes [*Pauluis*, 2011]. Analyzing the entropy budget of organized convection in both rotating and nonrotating frameworks may be useful in order to understand the self-aggregation process, particularly in light of the hypothesis that aggregation itself is temperature dependent [*Wing and Emanuel*, 2013; *Emanuel et al*., 2014]. The entropy budget of moist convection in an extremely warm atmosphere may also be of interest for future work given the failure of the scaling relations derived in section 4 to predict a closed entropy budget under these conditions. Such a study may have implications for our understanding of water-vapor-dominated atmospheres such as that postulated to have existed on Venus in its early history [e.g., *Kasting*, 1988].

Acknowledgments
We thank F. Laliberté and O. Pauluis for useful discussions and two anonymous reviewers for constructive comments. This work was supported by NSF grant AGS-1148594, and high-performance computing support from Yellowstone (ark:/85065/d7wd3xhc) was provided by NCAR's Computational and Information Systems Laboratory, sponsored by the NSF. We are grateful to G. Bryan for providing and maintaining CM1. CM1 is available at http://www2.mmm.ucar.edu/people/bryan/cm1/.

References

Allen, M. R., and W. J. Ingram (2002), Constraints on future changes in climate and the hydrologic cycle, *Nature*, *419*, 224–232.
Braun, S. A., and W.-K. Tao (2000), Sensitivity of high-resolution simulations of hurricane Bob (1991) to planetary boundary layer parameterizations, *Mon. Weather Rev.*, *128*, 3941–3961.
Bretherton, C. S., P. N. Blossey, and M. Khairoutdinov (2005), An energy-balance analysis of deep convective self-aggregation above uniform SST, *J. Atmos. Sci.*, *62*, 4273–4292.
Bryan, G. H., and J. M. Fritsch (2002), A benchmark simulation for moist nonhydrostatic numerical models, *Mon. Weather Rev.*, *130*, 2917–2928.
Bryan, G. H., and R. Rotunno (2009), The maximum intensity of tropical cyclones in axisymmetric numerical model simulations, *Mon. Weather Rev.*, *137*, 1770–1789.
Craig, G. C. (1996), Dimensional analysis of a convecting atmosphere in equilibrium with external forcing, *Q. J. R. Meteorol. Soc.*, *122*, 1963–1967.
Emanuel, K. (2000), Quasi-equilibrium thinking, in *General Circulation Model Development: Past, Present, and Future, International Geophysics*, vol. *70*, edited by D. A. Randall, pp. 225–255, Academic, San Diego, Calif.
Emanuel, K., A. A. Wing, and E. M. Vincent (2014), Radiative-convective instability, *J. Adv. Model. Earth Syst.*, *6*, 75–90, doi:10.1002/2013MS000270.
Emanuel, K. A., and M. Bister (1996), Moist convective velocity and buoyancy scales, *J. Atmos. Sci.*, *53*, 3276–3285.
Emanuel, K. A., J. D. Neelin, and C. S. Bretherton (1994), On large-scale circulations in convecting atmospheres, *Q. J. R. Meteorol. Soc.*, *120*, 1111–1143.
Fraedrich, K., and F. Lunkeit (2008), Diagnosing the entropy budget of a climate model, *Tellus. Ser. A*, *60*, 921–931.
Goody, R. (2000), Sources and sinks of climate entropy, *Q. J. R. Meteorol. Soc.*, *126*, 1953–1970.
Held, I. M., and B. J. Soden (2006), Robust responses of the hydrological cycle to global warming, *J. Clim.*, *19*, 5686–5699.
Johnson, D. R. (1997), "General coldness of climate models" and the Second Law: Implications for modeling the Earth system, *J. Clim.*, *10*, 2826–2846.
Kasting, J. F. (1988), Runaway and moist greenhouse atmospheres and the evolution of Earth and Venus, *Icarus*, *74*, 472–494.
Knietzsch, M.-A., A. Schröder, V. Lucarini, and F. Lunkeit (2015), The impact of oceanic heat transport on the atmospheric circulation, *Earth Syst. Dyn.*, *6*, 591–615.
Laliberté, F., J. Zika, L. Mudryk, P. J. Kushner, J. Kjellsson, and K. Döös (2015), Constrained work output of the moist atmospheric heat engine in a warming climate, *Science*, *347*, 540–543.
LeMone, M. A., and E. J. Zipser (1980), Cumulonimbus vertical velocity events in GATE. Part I: Diameter, intensity and mass flux, *J. Atmos. Sci.*, *37*, 2444–2457.
Lin, Y.-L., R. D. Farley, and H. D. Orville (1983), Bulk parameterization of the snow field in a cloud model, *J. Clim. Appl. Meteorol.*, *22*, 1065–1092.
Lucarini, V., K. Fraedrich, and F. Lunkeit (2010), Thermodynamic analysis of snowball Earth hysteresis experiment: Efficiency, entropy production and irreversibility, *Q. J. R. Meteorol. Soc.*, *136*, 2–11.
Pascale, S., J. M. Gregory, M. Ambaum, and R. Tailleux (2011), Climate entropy budget of the HadCM3 atmosphere-ocean general circulation model and of FAMOUS, its low-resolution version, *Clim. Dyn.*, *36*, 1189–1206.
Pauluis, O. (2011), Water vapor and mechanical work: A comparison of Carnot and steam cycles, *J. Atmos. Sci.*, *68*, 91–102.
Pauluis, O., and I. M. Held (2002a), Entropy budget of an atmosphere in radiative-convective equilibrium. Part I: Maximum work and frictional dissipation, *J. Atmos. Sci.*, *59*, 125–139.
Pauluis, O., and I. M. Held (2002b), Entropy budget of an atmosphere in radiative-convective equilibrium. Part II: Latent heat transport and moist processes, *J. Atmos. Sci.*, *59*, 140–149.
Pauluis, O., V. Balaji, and I. M. Held (2000), Frictional dissipation in a precipitating atmosphere, *J. Atmos. Sci.*, *57*, 989–994.
Peixoto, J. P., A. H. Oort, M. de Almeida, and A. Tomé (1991), Entropy budget of the atmosphere, *J. Geophys. Res.*, *96*, 10,981–10,988.
Raymond, D. J. (2013), Sources and sinks of entropy in the atmosphere, *J. Adv. Model. Earth Syst.*, *5*, 755–763, doi:10.1002/jame.20050.
Rennó, N. O., and A. P. Ingersoll (1996), Natural convection as a heat engine: A theory for CAPE, *J. Atmos. Sci.*, *53*, 572–585.
Robe, F. R., and K. A. Emanuel (1996), Moist convective scaling: Some inferences from three-dimensional cloud ensemble simulations, *J. Atmos. Sci.*, *53*, 3265–3275.
Romps, D. M. (2008), The dry-entropy budget of a moist atmosphere, *J. Atmos. Sci.*, *65*, 3779–3799.
Seeley, J. T., and D. M. Romps (2015), Why does tropical convective available potential energy (CAPE) increase with warming?, *Geophys. Res. Lett.*, *42*, 10,429–10,437, doi:10.1002/2015GL066199.

Siebesma, A. P., and H. J. J. Jonker (2000), Anomalous scaling of cumulus cloud boundaries, *Phys. Rev. Lett.*, *85*, 214–217.
Singh, M. S. (2014), The response of moist convection and the atmospheric general circulation to climate warming, PhD thesis, Mass. Inst. of Technol., Cambridge.
Singh, M. S., and P. A. O'Gorman (2013), Influence of entrainment on the thermal stratification in simulations of radiative-convective equilibrium, *Geophys. Res. Lett.*, *40*, 4398–4403, doi:10.1002/grl.50796.
Singh, M. S., and P. A. O'Gorman (2014), Influence of microphysics on the scaling of precipitation extremes with temperature, *Geophys. Res. Lett.*, *41*, 6037–6044, doi:10.1002/2014GL061222.
Singh, M. S., and P. A. O'Gorman (2015), Increases in moist-convective updraught velocities with warming in radiative-convective equilibrium, *Q. J. R. Meteorol. Soc.*, *141*, 2828–2838.
Stephens, G. L., and D. M. O'Brien (1993), Entropy and climate. I: ERBE observations of the entropy production of the earth, *Q. J. R. Meteorol. Soc.*, *119*, 121–152.
Wing, A. A., and K. A. Emanuel (2013), Physical mechanisms controlling self-aggregation of convection in idealized numerical modeling simulations, *J. Adv. Model. Earth Syst.*, *6*, 59–74, doi:10.1002/2013MS000269.
Wing, A. A., S. J. Camargo, and A. H. Sobel (2016), Role of radiative-convective feedbacks in spontaneous tropical cyclogenesis in idealized numerical simulations, *J. Atmos. Sci.*, doi:10.1175/JAS-D-15-0380.1, in press.
Woollings, T., and J. Thuburn (2006), Entropy sources in a dynamical core atmosphere model, *Q. J. R. Meteorol. Soc.*, *132*, 43–59.